

MOF-Based Polymeric Nanocomposite Films as Potential Materials for Drug Delivery Devices in Ocular Therapeutics

J. Gandara-Loe,¹ B. E. Souza,¹ A. Missyul, G. Giraldo, J.-C. Tan, and J. Silvestre-Albero*



Cite This: *ACS Appl. Mater. Interfaces* 2020, 12, 30189–30197



Read Online

ACCESS |



Metrics & More



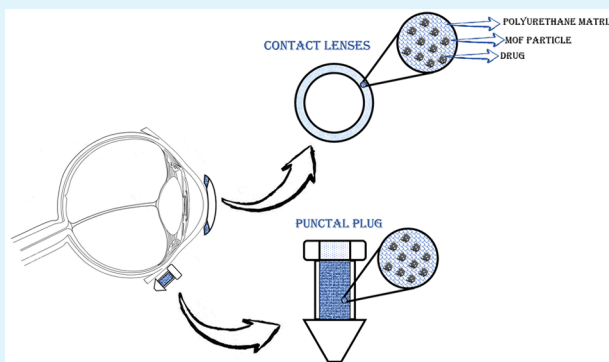
Article Recommendations



Supporting Information

ABSTRACT: Novel MOF-based polymer nanocomposite films were successfully prepared using Zr-based UiO-67 as a metal–organic framework (MOF) and polyurethane (PU) as a polymeric matrix. Synchrotron X-ray powder diffraction (SXRPD) analysis confirms the improved stability of the UiO-67 embedded nanocrystals, and scanning electron microscopy images confirm their homogeneous distribution (average crystal size ~ 100 – 200 nm) within the $50 \mu\text{m}$ thick film. Accessibility to the inner porous structure of the embedded MOFs was completely suppressed for N_2 at cryogenic temperatures. However, ethylene adsorption measurements at 25°C confirm that at least 45% of the MOF crystals are fully accessible for gas-phase adsorption of nonpolar molecules. Although this partial blockage limits the adsorption performance of the embedded MOFs for ocular drugs (e.g., brimonidine tartrate) compared to the pure MOF, an almost 60-fold improvement in the adsorption capacity was observed for the PU matrix after incorporation of the UiO-67 nanocrystals. The UiO-67@PU nanocomposite exhibits a prolonged release of brimonidine (up to 14 days were quantified). Finally, the combined use of SXRPD, thermogravimetric analysis (TGA), and Fourier transform infrared (FTIR) analyses confirmed the presence of the drug in the nanocomposite film, the stability of the MOF framework and the drug upon loading, and the presence of brimonidine in an amorphous phase once adsorbed. These results open the gate toward the application of these polymeric nanocomposite films for drug delivery in ocular therapeutics, either as a component of a contact lens, in the composition of lacrimal stoppers (e.g., punctal plugs), or in subtenon inserts.

KEYWORDS: brimonidine, MOFs, polyurethane, ocular plugs, drug delivery



1. INTRODUCTION

Glaucoma is a pathological eye disorder associated with an increase in the intraocular pressure (IOP) and one of the leading causes of irreversible blindness worldwide.¹ Approximately, 70 million middle-aged people and elderly are affected by its common form, open-angle glaucoma whereof 10% ends in bilateral blindness.² Among the different drugs to treat glaucoma, brimonidine tartrate is one of the most widely applied. Brimonidine is an α -adrenergic agonist able to reduce the ocular pressure through a constriction in the blood vessels, ending in the decrease of aqueous humor production.³

Conventional drug delivery systems such as eye droplets represent 90% of the marketed ophthalmic formulations.^{4,5} However, severe constraints are associated with this topical approach such as tear turnover, fast nasolacrimal drainage, and reflex blinking, thus ending in a nonoptimal dosage.⁶ Roughly, only 5% of the drug applied topically reaches the deeper ocular tissues, thus forcing pharmaceutical producers to increase the drug concentration, with the associated increase in the toxicity and, indirectly, the risk of side effects.⁷ Another limitation of these topical administration routes is the low compliance of patients, mainly elderly, to strictly follow the administration

protocol (administration of a number of droplets several times per day).

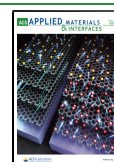
The development of more efficient ocular drug delivery systems with well-designed and prolonged release kinetics remains a challenge in materials science and ophthalmology. Nanocarriers such as poly(acrylic acid) nanoparticles,⁸ chitosan nanoparticles,⁹ nanovesicles,¹⁰ and layered double hydroxides (LDHs)¹¹ have been reported as promising alternatives for topical brimonidine dosage. However, the main limitation of some of these materials for potential application falls in the physical (low gravimetric capacity for the drug) and textural properties.

Novel drug administration platforms to treat ocular disorders prepared from polymeric materials (solid or semisolid inserts) have gained large popularity in the last few

Received: April 23, 2020

Accepted: June 12, 2020

Published: June 12, 2020



years.^{12–14} The potential advantage of these polymeric devices is the accurate dosing, increased ocular residence time, reduction of systemic side effects, or better patient compliance, just to mention some.¹⁵ Due to the potential of these devices in ocular drug delivery, several companies have patented and commercialized them. For instance, one of the first marketed ocular inserts has been commercialized by Alza (Vacville, CA) as Ocusert, which is used to dose antiglaucoma drug pilocarpine for a maximum of 5–7 days.^{16,17} Although these are excellent numbers, the absence of a well-defined regular three-dimensional (3D) network within these polymeric matrices limits their total drug uptake and hinders the controlled release.

Based on these premises, the design of novel functional ocular polymeric devices through the incorporation of perfectly designed high-capacity nanofillers would be a key stepping stone to increase the versatility and impact of these inserts in nanomedicine. A potential approach not widely explored in the literature could be the incorporation of nanocarriers with improved drug adsorption uptake and controlled release, provided that the incorporated guest structures do not alter the mechanical properties of the insert, while the porous structure of the nanofiller remains fully accessible in the mixed formulation.^{18–20} Among the potential candidates, high-surface-area porous materials such as metal–organic frameworks (MOFs) provide an avenue to achieve these requirements.²¹ MOFs are crystalline materials formed by the union of metal centers and organic linkers. The self-assembly of metal clusters (or nodes) and organic ligands allows the design of a large number of one-dimensional (1D) to 3D networks characterized by high surface area, large pore volume, and tuneable host–guest interactions.²² Over the last few years, these materials have shown promise as a potential platform for drug delivery in the powder form.^{23,24} Recent studies from Gandara-Loe et al. have shown that MOFs can store a large amount of brimonidine tartrate (up to 600 mg of drug per gram of MOF), with an extended release time of up to 12 days, in the specific case of UiO-67. Furthermore, *in vitro* cytotoxicity assays have demonstrated the low toxicity of UiO-67 for retinal photoreceptor cells.²⁵ The excellent performance of UiO-67 is motivated by the presence of large tetrahedral and octahedral cages in the micro/mesoporous range.²⁶ Taking into account these excellent properties, the successful incorporation of these 3D porous networks in continuous polymeric matrices will offer a new perspective in nanomedicine with more suitable nanocomposite materials (instead of working with powders), with novel functionalities (e.g., drug delivery properties), to be used either as microinserts (e.g., punctal plugs in lacrimal or subtenon cavities) or as a component in contact lenses.^{27,28}

Polymer–MOF nanocomposite materials have already been reported in the literature as potential candidates for gas adsorption/separation processes such as CO₂/N₂ or CO₂/CH₄ separation or ethylene adsorption.^{29,30} There are recent studies on the use of HKUST-1/polyurethane nanocomposite membranes for drug encapsulation and controlled release.³¹ However, the understanding of molecular accessibility in liquid-phase adsorption processes is still a challenge due to the different nature of the polymeric network and the MOF nanofiller. To the best of our knowledge, polymer–MOF nanocomposite films have not yet been tested as a drug delivery carrier for ocular therapeutics.

Based on these premises, the main goal of this work is to report an optimal synthesis of functional MOF-based polyurethane thin films and to evaluate the performance of these UiO-67@PU nanocomposites for brimonidine adsorption/release in the liquid phase. The successful development of these functional materials (MOF@polymer) will open the gate toward the application of these devices in a number of ocular disorders that require a controlled and prolonged release of drugs, from glaucoma treatment to postsurgical treatments by anti-inflammatory drugs.

2. EXPERIMENTAL SECTION

2.1. UiO-67 Synthesis. UiO-67 was synthesized based on the procedure reported in the literature by Katz et al.³² Briefly, 0.268 g of ZrCl₄ was dissolved in a mixture of 20 mL of *N,N*-dimethylformamide (DMF) and 2 mL of concentrated HCl. In a second vessel, 0.360 g of 4,4'-biphenyldicarboxylic acid (BDPC) was dissolved in 40 mL of DMF. The two solutions were mixed and maintained under sonication for 30 min. The final solution was transferred to a 200 mL glass jar, closed tightly, and kept at 80 °C overnight. The resulting white solid was filtered and washed first with DMF (2 × 30 mL) and then with ethanol (2 × 30 mL). The sample was activated first under low vacuum conditions (13 × 10⁻³ Pa) up to 90 °C and, afterward, at 150 °C for 3 h under ultrahigh vacuum conditions.

2.2. UiO-67@PU Synthesis. The UiO-67@PU nanocomposite films were fabricated by following the procedures described below. Polyurethane (PU) solution was prepared by dissolving poly[4,4'-methylenebis(phenyl isocyanate)-alt-1,4-butanediol/di(propylene glycol)/polyurethane] pellets (purchased from Sigma-Aldrich and used without further alterations) in tetrahydrofuran (THF) for 24–48 h until complete dissolution of polymer pellets. UiO-67@PU nanocomposites (30 wt %) and pristine PU films were produced by the dispersion of a specified amount of previously synthesized MOF particles (of a required weight percent) in a small amount of THF (930 mg of MOF per 1 mL of THF) before their incorporation in the PU-THF solution. The dispersion was performed by a combination of sonication (5 min) and magnetic stirring (20 min, 80 rpm). This strategy, followed by Cohen et al.,³³ has proven to be a versatile approach for the preparation of homogeneous polymer–MOF nanocomposites. The thin films were subsequently cast onto a glass substrate via the doctor blade technique using a casting speed of 10 mm/s to achieve membranes of ~50 μm in thickness.^{30,34}

2.3. Synchrotron X-Ray Powder Diffraction (SXRPD) Analysis. Synchrotron X-ray powder diffraction (SXRPD) data were collected at the powder diffraction end station of the MSPD beamline at synchrotron ALBA in Spain using a MYTHEN detector and a wavelength of 0.4227 Å. SXRPD measurements were performed at 25 °C for the as-synthesized UiO-67, PU, and the UiO-67@PU films, and also for the UiO-67@PU films after brimonidine adsorption. The reference spectra for brimonidine tartrate powder was also determined.

2.4. Thermogravimetric Analysis (TGA). Thermogravimetric analysis data for UiO-67, PU film, and UiO-67@PU film were obtained using a TG-DTA METTLER TOLEDO equipment model TG/SDTA851e/SF/1100. The samples were measured using an alumina sample holder and a temperature range of 25–600 °C at a heating rate of 5 °C/min under N₂ flow.

2.5. Scanning Electron Microscopy (SEM) Evaluation. Cross-sectional micrographs were recorded using a Hitachi scanning electron microscope model S3000N. This microscope is equipped with a Bruker brand X-ray detector (model Xflash 3001) for energy-dispersive spectroscopy (EDS) microanalysis and mapping. Samples were kept under cryogenic conditions (liquid N₂) before the analysis to obtain a high-quality cross section and avoid surface alterations during the sectioning process.

2.6. Nitrogen and Ethylene Adsorption/Desorption Isotherms. The textural properties and gas-phase accessibility of the different samples were evaluated by gas physisorption, i.e., nitrogen adsorption at -196 °C and ethylene adsorption at 25 °C. Nitrogen

gas adsorption measurements were performed in a homemade fully automated manometric equipment designed and constructed by the Advanced Materials Group (LMA), now commercialized as N2GSorb-6 (Gas to Materials Technologies, www.g2mtech.com). Nitrogen adsorption data were used to calculate (a) the total pore volume (V_t) at a relative pressure of 0.95, (b) the Brunauer–Emmett–Teller (BET) surface area (S_{BET}), and (c) the micropore volume (V_{N_2}), after application of the Dubinin–Radushkevich (DR) equation. Ethylene adsorption experiments were performed in a homebuilt fully automated manometric equipment, now commercialized by Quantachrome Corp. as VSTAR. Before the experiments, the samples were degassed at 100 °C for 8 h under high vacuum conditions (10^{-5} torr).

2.7. Loading and Release Experiments. Brimonidine tartrate quantification was done based on the high-performance liquid chromatography method developed by Karamanos et al.³⁵ A stock solution of 1500 ppm of brimonidine tartrate was prepared by dissolving 1.5 g in 1000 mL of ultrapure water. The calibration curve was constructed by measuring concentrations from 2 to 15 ppm using chromatographic conditions, an analytical column Supelcosil LC-18, 5 μm , 250×4.6 mm² i.d. stainless steel (Supelco, Bellefonte, PA) equipped with an RP-18 precolumn, 20×4.6 mm² i.d. (Supelco). The mobile phase was a 9:1 (v/v) mixture of 10 mM triethylamine pH 3.2 buffer and acetonitrile. The separation was performed at room temperature, at a flow rate of 1.0 mL/min, an injection volume of 20 μL , and the detection of brimonidine at 248 nm.

2.7.1. Brimonidine Loading Experiments. Brimonidine adsorption isotherms were performed at 25 °C using a series of aqueous solutions (pH = 7) with initial concentrations of 250, 500, 750, 1000, and 1500 ppm of brimonidine tartrate. The nanocomposite films were degassed at 100 °C overnight before the experiment. Approximately 100 mg of film was placed in contact with 50 mL of solution at each of the concentrations described above and left under stirring until equilibrium had reached. Aliquots were taken at different time intervals to evaluate the adsorption kinetics of the films.

The quantification of brimonidine was determined using high-performance liquid chromatography (HPLC) by diluting each aliquot 1:100 and using the method described above.

2.7.2. Brimonidine Release Experiments. The UiO-67@PU film (100 mg), previously degassed, was loaded with brimonidine by contacting it with 50 mL of 1500 ppm brimonidine tartrate aqueous solution. The system was left at 25 °C under stirring for 24 h to ensure full equilibrium. After this time, the film was separated from the solution and an aliquot was taken to determine the maximum loading amount. The brimonidine-loaded film was washed several times with ultrapure water and dried under vacuum at 60 °C for 6 h. The dried brimonidine-loaded film was immersed in 50 mL of physiological solution (phosphate-buffered saline, PBS), and aliquots were taken at different times up to 14 days. The aliquots were diluted 1:1000, and brimonidine quantification was performed using the HPLC method described above.

3. RESULTS AND DISCUSSION

3.1. Characterization of the Synthesized Films and Accessibility of the Embedded MOFs. The crystallinity of the synthesized materials has been evaluated through synchrotron X-ray powder diffraction (SXRPD) measurements. Figure 1 shows the comparative SXRPD patterns for the as-synthesized UiO-67 crystals, obtained by the solvothermal method, and the UiO-67@PU film. The SXRPD pattern of the UiO-67 sample perfectly fits with the simulated pattern and with those described previously in the literature, thus confirming the quality and reproducibility of the synthesized MOF.³² Concerning the UiO-67@PU nanocomposite material, the SXRPD pattern confirms the presence of a semicrystalline system, with the combination of crystallinity due to UiO-67 nanoparticles and the amorphous background from the PU matrix. The PU matrix is characterized by a broad peak at 2θ

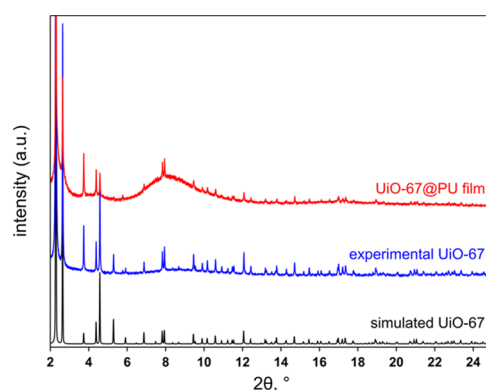


Figure 1. Synchrotron XRPD experimental patterns of UiO-67 and UiO-67@PU films accompanied by the simulated pattern of UiO-67.

between 6 and 12° (see Figure S1), whereas the main diffraction peaks of the MOF can be clearly appreciated at $2\theta = 2.3\text{--}2.6^\circ$. These results confirm the preservation of the 3D network in the UiO-67 nanocrystals upon incorporation in the polymeric matrix and their excellent crystallinity.

Morphologically, the UiO-67@PU film is a semitransparent and flexible composite material (Figure S2) with high versatility for the production of different ocular devices. As shown in Figure 2, the nanocomposite film is formed by MOF

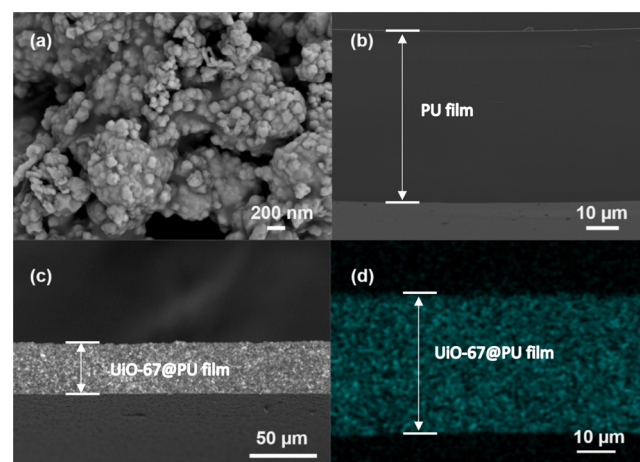


Figure 2. SEM micrograph of (a) as-synthesized UiO-67 nanocrystals, (b) cross section of a 50 μm thick neat PU film, (c) cross section of the 50 μm UiO-67@PU film, and (d) Zr EDX mapping (green color) of a cross section of the UiO-67@PU nanocomposite film.

nanocrystals (average crystal size 100–200 nm) embedded in the polyurethane matrix, giving a film of approximately 50 μm thickness. Figure 2c shows the relatively uniform distribution of the UiO-67 nanocrystals within the PU matrix, an observation that was further confirmed by specific Zr-mapping experiments (Figure 2d). Previous results described in the literature for gas separation using similar composites have anticipated that the accessibility (permeation of gases) decreases with the thickness of the film.^{34,36} Based on this assumption and taking into account the objectives of this study (liquid-phase adsorption processes usually possess lower kinetics compared to gas adsorption processes), we assume that a 50 μm film can be considered as a good approach. Furthermore, 30 wt % MOF loading can be considered as an upper limit to keep a good balance between the thermome-

chanical and toughness properties for a potential future application.^{34,37}

Thermogravimetric (TGA) analyses were used to evaluate the thermal stability of the nanocomposite film compared to those of the pure components (PU and UiO-67). Polyurethane and UiO-67 nanoparticles exhibit characteristic decomposition profiles with very sharp and symmetric decomposition peaks, as shown in Figure 3. For instance, the pure PU film exhibits a

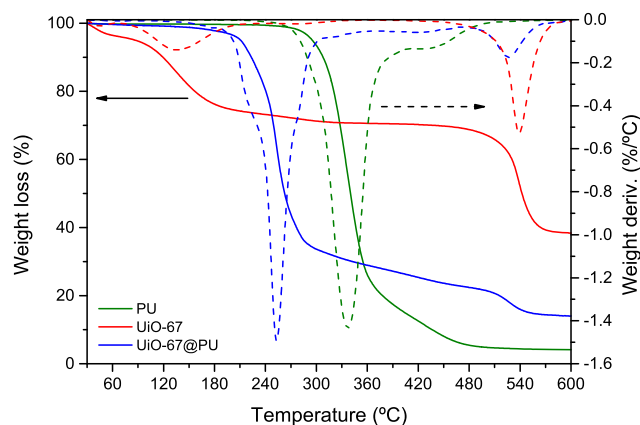


Figure 3. Thermogravimetric analysis (TGA and DTGA) of PU, UiO-67, and UiO-67@PU films.

decomposition profile with a well-defined decomposition peak centered at 337 °C and a small shoulder at 430 °C, which is typical of polyurethane materials.³⁸ In the case of UiO-67, the TGA profile shows the release of the solvent at 135 °C and the main framework decomposition close to 550 °C.²⁶ Figure 3 also shows the TGA profile of the UiO-67@PU nanocomposite film. In this case, the scenario is more complex. As can be seen, the nanocomposite material exhibits a broad decomposition profile with the main peak located between 200 and 300 °C. Interestingly, this peak is not symmetric and clear shoulders can be seen at around 217 and 278 °C, in addition to the main contribution at 252 °C. Taking into account that 70 wt % of the composite corresponds to PU, the main contribution at 252 °C must be attributed to the decomposition of the polymeric matrix. Compared to the pure polymer (ca. 337 °C), these results indicate a clear shift to lower temperatures upon incorporation of the MOF nanofillers, in close agreement with previous studies reported in the literature.³⁴ Apparently, the incorporation of the MOF nanocrystals limits the cross-linking between PU molecular chains, thus reducing their thermal stability. For the sake of clarity, a deconvolution of the DTGA profile for the nanocomposite system can be seen in Figure S3. In addition to the decomposition of the polymeric matrix, the aforementioned shoulders must be attributed to solvent removal (ca. 217 °C) and to the secondary contribution in the decomposition of the PU matrix (ca. 278 °C). Furthermore, the nanocomposite material exhibits an additional decomposition peak at 528 °C, unambiguously attributed to the degradation of the embedded MOF. This finding constitutes another proof about the successful incorporation of the MOF crystals in the polymeric matrix. Table S1 contains a summary of the TGA results for the three samples evaluated.

To check the accessibility of the 3D porous network in UiO-67@PU nanocomposite films to gas molecules, the nitrogen adsorption/desorption isotherm was performed at −196 °C

and compared to that of the pure MOF. As can be seen in Figure S4, UiO-67 presents the typical adsorption–desorption isotherm already described elsewhere,³² with a large uptake at low relative pressures due to its highly microporous framework and the associated step at $p/p_0 \sim 0.15$ attributed to the presence of wider pores (small mesopores). This observation is in close agreement with the presence of two kinds of cavities in UiO-67, tetrahedral and octahedral cages with diameters of 1.1 and 2.3 nm, respectively.³² Interestingly, in the specific case of the UiO-67@PU film, the accessibility for nitrogen at cryogenic temperatures is completely suppressed over the whole relative pressure range evaluated. This observation is in close agreement with previous studies described in the literature for ZIF-8- and ZIF-7-loaded polymeric matrices.³⁷ Apparently, nitrogen with a quadrupolar moment is not able to diffuse through the rubbery polymeric network at cryogenic temperatures. Despite the inaccessibility of nitrogen to the embedded MOF crystals, this observation does not necessarily reflect the real scenario in the composite material. Based on our previous experience, adsorption of nonpolar molecules (for instance, hydrocarbons) constitutes a complementary tool to evaluate the porous structure in these MOF@polymer nanocomposites. Figure 4 shows the ethylene adsorption/

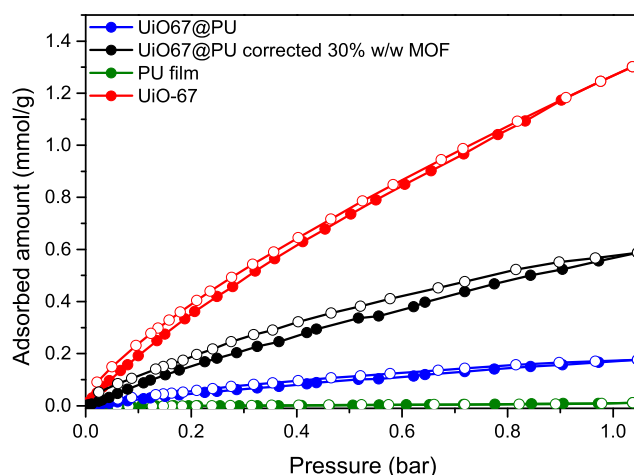


Figure 4. Ethylene adsorption (filled symbol)–desorption (open symbol) isotherms at 25 °C in as-synthesized UiO-67, PU, and UiO-67@PU films.

desorption isotherms at 25 °C for pure PU, UiO-67, and the nanocomposite. These results show that, contrary to N₂, ethylene is indeed able to access the inner porous structure in this kind of materials. Whereas the pure PU film exhibits an adsorption capacity close to 0 mmol/g, UiO-67 nanoparticles are able to adsorb up to 1.31 mmol/g at a pressure of 1 bar. For the UiO-67@PU nanocomposite sample, the total adsorption capacity for ethylene at 1 bar is ca. 0.18 mmol/g. After normalization to the total amount of MOF (considering that the composite contains ca. 30 wt %), this value scales up to a total uptake of 0.59 mmol/g_{MOF}. Compared to pure UiO-67, this result constitutes a reduction of 55% in the adsorption capacity of the embedded crystals, i.e., embedded nanocrystals are indeed accessible to gas molecules, although only partially.

3.2. Brimonidine Adsorption and Release. Brimonidine adsorption isotherms were performed in aqueous media (ultrapure water) and at room temperature to quantify the maximum amount of drug adsorbed in the porous structure of

the synthesized films. As shown in Figure 5, while the adsorption in the pure PU film is close to 0 mg/g, the

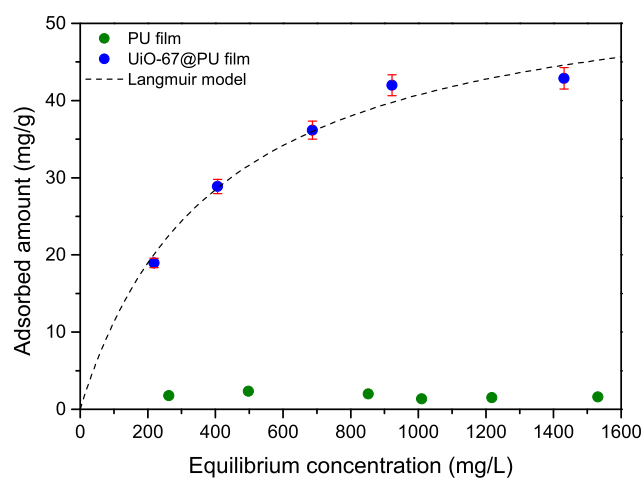


Figure 5. Brimonidine liquid-phase adsorption isotherms in PU and UiO-67@PU films at 25 °C ($C_0 = 1500$ ppm).

maximum brimonidine adsorption capacity in the UiO-67@PU film (at an equilibrium time of 4 h; see Figure S5) obtained from the Langmuir model achieves a value of 58.4 mg of brimonidine per gram of film, i.e., 194.7 mg of brimonidine per gram of UiO-67 (considering the nominal value of 30 wt % of UiO-67 in the film). This value differs from that reported in the literature for pure UiO-67 nanoparticles (ca. 600 $\text{mg}_{\text{brimonidine}}/\text{g}_{\text{MOF}}$).²⁵ The reduction in the adsorption capacity for the nanocomposite (around 67% reduction) is in close agreement with the gas-phase ethylene adsorption measurements described above (ethylene was able to access 45% of the porosity, whereas brimonidine only 32.5% of the MOF porous network). Although these numbers must be optimized, this finding constitutes an important development elucidating the potential application of these MOF-doped polymeric matrices for liquid-phase adsorption/desorption processes. Even though these processes are performed in the presence of a solvent (for instance, an aqueous solution), the embedded MOFs are able to preserve similar accessibility to the target molecule (e.g., ocular drug), compared to similar measurements in the gas phase, i.e., in the absence of the solvent. These results suggest that UiO-67 cavities are able to host both ethylene (molecular size of $4.7 \times 9.8 \text{ \AA}^2$) and brimonidine ($3.28 \times 4.18 \times 4.84 \text{ \AA}^3$) in a similar extend.^{39,40} Compared to the neat PU polymer, the incorporation of UiO-67 nanofillers gives rise to a 60-fold increase in the adsorption capacity for brimonidine tartrate.

To mimic a potential application in the human body, brimonidine release isotherms were performed in the PBS solution at room temperature and neutral pH, Figure 6. As can be observed, the UiO-67@PU nanocomposite exhibits a fast release (up to 7% of the total uptake) in the first minutes of the experiment. Afterward, there is a continuous release with time up to a maximum of 10% of the total brimonidine retained after 14 day exposure. The large release in the first few hours must be attributed to brimonidine weakly interacting with the nanocomposite and/or adsorbed in the external layers/pores of the film. Considering the traditional topical administration of brimonidine a patient must take one droplet of brimonidine solution of 2 mg/mL (Alphagan P, Allergan) every 8 h, which means 0.3 mg of brimonidine per day or 4.2 mg in 14 days.⁷

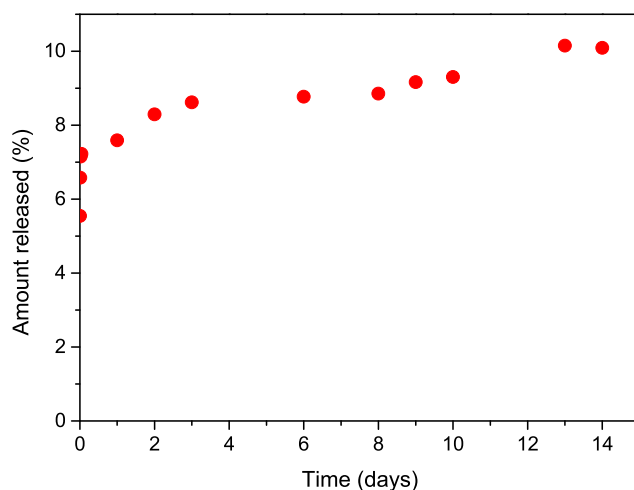


Figure 6. Brimonidine tartrate release kinetics at 25 °C in physiological media PBS (loading concentration 1500 ppm).

Taking into account the total uptake of 58.4 mg/g for our composite, a release of 10% (5.8 mg/g) after 14 days is within the needs of a normal patient with glaucoma, thus validating our approach. At this point, it is important to highlight that we cannot exclude the possibility that some brimonidine is already removed/released from the loaded film during the washing step performed after the loading and before the release experiment (this washing step was designed to remove exclusively the brimonidine retained in the external surface of the film).

At this point, the open questions remain the compatibility of the drug with the composite, the stability of the MOF structure after the loading process, and finally the potential location of the drug molecule in the composite system. The next sections are devoted to answering all of these questions.

3.3. Brimonidine–Composite Compatibility and Stability Studies. The structural stability of the MOF framework is an important parameter to be considered in liquid-phase adsorption processes. It is widely accepted in the literature that MOF materials can exhibit limited stability in the presence of aqueous environments or after the incorporation of the drug.⁴¹ In the specific case of UiO-67, it is well known that upon exposure to water or moisture, this system exhibits a large instability due to the hydrolysis of the linker–metal bonds and the associated pore collapse.^{42–44} However, the partial amorphization of the UiO-67 nanoparticles during the adsorption/release of brimonidine has been very useful to extend the released kinetics beyond 12 days, as described before by some of us.²⁵

In addition to structural stability, another concern is the adsorption mechanism. Adsorption of brimonidine into MOF-based polymeric films can be explained via three potential scenarios. As summarized in Figure 7, brimonidine can be adsorbed only in those MOF crystals located in the periphery of the PU film (option a), it can be adsorbed only in the polymeric matrix, i.e., MOF nanocrystals are completely blocked (option b), or it can be adsorbed equally in the different crystals homogeneously distributed within the PU film (option c). To identify which of these options is the most plausible to explain the adsorption mechanism, the UiO-67@PU nanocomposite has been thoroughly evaluated before and after adsorption of brimonidine using synchrotron X-ray

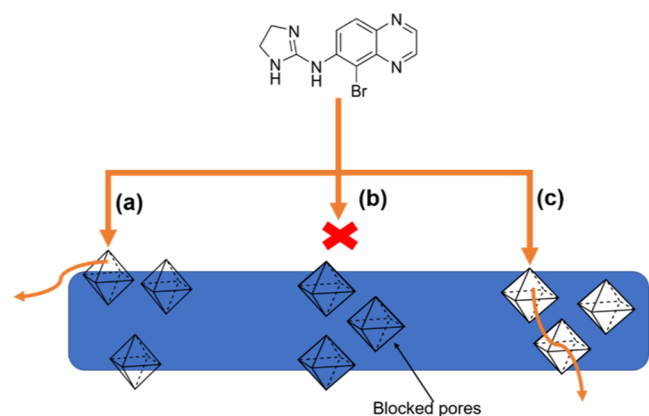


Figure 7. Scheme of possible scenarios for brimonidine adsorption in MOF@polymer composites: (a) adsorption in the peripheric MOF crystals and (b) fully inaccessible and (c) fully accessible embedded MOF nanocrystals.

diffraction, thermogravimetry (TGA), and Fourier transform infrared (FTIR).

Synchrotron X-ray diffraction measurements were performed to elucidate the structural parameters of the UiO-67 embedded crystals before and after the loading of brimonidine. As can be observed in Figure 8, both patterns are rather similar

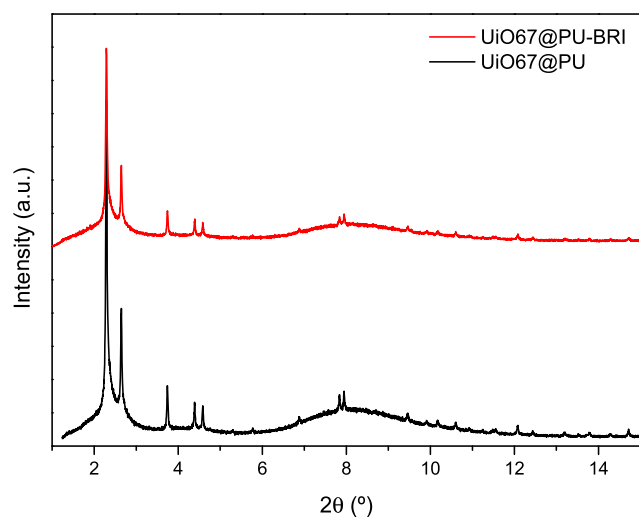


Figure 8. Synchrotron X-ray powder diffraction patterns of the UiO-67@PU film before and after being exposed to the brimonidine solution.

even after exposure to the brimonidine aqueous solution for several days. These results are contrary to the performance of pure MOF (Figure S6), where a significant structural deterioration was identified after 1 day in contact with water and confirms the improved structural stability of UiO-67 upon encapsulation in the PU matrix.²⁵

Although the cavities in UiO-67 (octahedral of 2.3 nm and tetrahedral of 1.15 nm) are large enough to accommodate the brimonidine molecule, the open question at this point is how to ascertain if brimonidine is able to take advantage of these cavities.³² Synchrotron X-ray diffraction measurements of the pure brimonidine tartrate (Figure S7) show a rich XRD pattern with a large number of peaks in the range between 2 and 18°, confirming the high crystallinity of this molecule. The absence of these peaks in the SXRPD pattern of the brimonidine-

loaded UiO-67@PU nanocomposite (Figure 8) could be a priori evidence of the absence of brimonidine both in the polymeric network and embedded MOF nanocrystals. However, this observation would be in contradiction with brimonidine adsorption measurements reported in Figure 5. This inconsistency must be explained due to amorphization of the drug upon adsorption, thus explaining the absence of peaks in the SXRPD pattern. This hypothesis would be in agreement with the encapsulation of the drug in the MOF cavities, with the associated limitation for these molecules to arrange in a periodic fashion. These conclusions are also supported by previous studies dealing with the adsorption/release of brimonidine through ocular devices, suggesting the transformation of crystalline brimonidine into an amorphous phase once it is adsorbed onto the material.^{45–47}

The unit cell parameters deduced for the embedded UiO-67 crystals after the Rietveld refinement are summarized in Table 1. Pure UiO-67 crystals have a cubic unit cell with lattice

Table 1. Summary of Structural Parameters and Adsorption Performance of UiO-67 and UiO-67@PU Films Before and After Loading with Brimonidine

	UiO-67	UiO-67@PU	UiO-67@PU-BRI
cell parameter, <i>a</i> (Å)	26.8447(9)	26.8306(6)	26.8252(6)
<i>S</i> _{BET} (m ² /g)	2614	0	
ethylene adsorption (mmol/g)	1.31	0.18	
brimonidine adsorption (mg/g)	600 ²⁵	58.4	
brimonidine release (%)	50% (12 days)	10% (14 days)	

parameters $a = b = c = 26.8447(9)$ Å. As can be observed, the lattice parameters remain rather similar after incorporation of the UiO-67 crystals in the polymeric matrix, in close agreement with the high quality of the crystals described in Figure 1. Interestingly, lattice parameters do not change after exposure of the UiO-67@PU nanocomposite to an aqueous solution of brimonidine. Although these results confirm the large stability of UiO-67 nanocrystals in an aqueous environment upon incorporation in the PU matrix, these are not conclusive about the location of brimonidine upon adsorption. Unfortunately, Rietveld refinement analysis of the embedded crystals does not allow us to answer this question due to the limited quality of the SXRPD pattern.

To further ascertain the adsorption mechanism, TGA analysis was performed for the UiO-67@PU film after the loading of brimonidine. For clarity, the TGA of pure brimonidine tartrate is included in Figure S8. Brimonidine tartrate exhibits a single decomposition peak at around 210 °C. A closer look to the TGA profile for the brimonidine-loaded UiO-67@PU nanocomposite (Figure S9) shows that the TGA peaks corresponding to the decomposition of the PU matrix and the UiO-67 crystals are shifted to higher temperatures upon adsorption. In addition, the thermogram shows an additional tiny peak at 210 °C, not present in the unloaded UiO-67@PU material, which can be attributed to brimonidine within the composite film (blue peak deconvoluted in Figure S10). Although the shifts observed in Figure S9 for the decomposition of PU and UiO-67 upon brimonidine adsorption could be an indication of the presence of brimonidine in both domains, the real location of the drug remains an open question. Last but not least, it is important to

highlight that the quantification of the tiny peak at 210 °C corresponds to $\sim 23 \text{ mg}_{\text{brimonidine}}/\text{g}_{\text{composite film}}$. Although this is a rough estimation, we cannot exclude that around 60% of the brimonidine loaded at 1500 ppm (Figure 5) could be lost during the washing step when applied before the TGA analysis. A similar hypothesis could be used to explain the low release achieved in Figure 6.

Finally, the presence of the drug has been evaluated using FTIR of the UiO-67@PU film before and after loading with brimonidine, Figure 9. The FTIR spectra of the individual

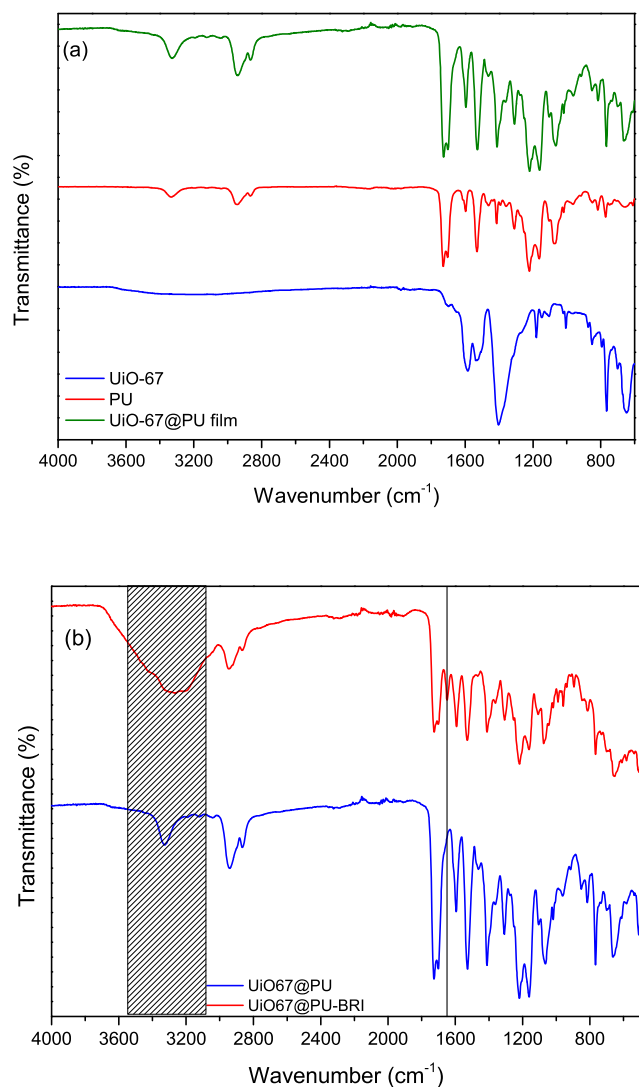


Figure 9. FTIR spectra of (a) UiO-67 (bottom), PU (middle), and UiO-67@PU (upper) films and (b) UiO-67@PU film before (bottom) and after (upper) loading with brimonidine.

components have also been included for clarity. As can be observed, before loading, the FTIR spectra of the UiO-67@PU film shows the characteristic peaks of PU and UiO-67. PU has a characteristic peak at 3329 cm^{-1} attributed to the stretching of the NH bond (Figure 9a). In addition, there are two contributions at 1724 and 1696 cm^{-1} due to the poly-(caprolactone) ester bond and the $-\text{CH}$ stretching vibration at 2944 cm^{-1} , among others.^{48,49} The characteristic peaks of UiO-67 can be observed at 1594 , 1528 , and 1411 cm^{-1} due to the stretching vibrations of the carboxylate group of the ligands

and the peaks at 815 , 766 , and 652 cm^{-1} due to the Zr–O stretching vibrations.^{50,51}

As already reported in the literature, brimonidine tartrate also presents characteristic vibrations in the IR range. These characteristic vibrations include peaks at 3212 and 3268 cm^{-1} owing to the N–H stretching vibration from the secondary amine groups ($\text{RR}'\text{-NH}$). The peak at around 1650 cm^{-1} is attributed to C=O stretching, and the peak at 1284 cm^{-1} is attributed to $-\text{CN}$ stretching.^{52–54}

The most remarkable feature of the FTIR spectra of UiO-67@PU after loading brimonidine is, in addition to the bands described above due to PU and UiO-67, the presence of a wide contribution at around $3575\text{--}3074 \text{ cm}^{-1}$. This broad contribution could be associated to the overlapping of signals from adsorbed H_2O (O–H stretching at 3404 cm^{-1}) and to the stretching $-\text{NH}$ vibrations characteristics of urea and urethane bonds (3333 cm^{-1}) in PU.^{48,49} However, taking into account that the brimonidine-loaded sample has been vacuum-dried at $60 \text{ }^\circ\text{C}$ before the FTIR spectra, and the absence of this wide contribution in the drug-free nanocomposite film, the presence of this broad contribution must be unambiguously attributed to the presence of brimonidine chemically interacting with the composite via hydrogen bonding with surface oxygen and nitrogen groups. This finding is supported by the presence of a new peak at 1650 cm^{-1} (solid line in Figure 9b) in the loaded film due to the C=O groups of the brimonidine tartrate. These assignments are in perfect agreement with previous studies on $\text{NH}_2\text{-MIL-88(Fe)}$ loaded with brimonidine.⁵³ In summary, FTIR spectra clearly confirm the presence of the drug in the UiO-67@PU film, although the real location, either in the polymeric matrix or in the UiO-67 network, cannot be easily identified.

4. CONCLUSIONS

We have successfully developed a novel UiO-67-based polyurethane film with an excellent adsorption/release performance for an ocular drug such as brimonidine tartrate. Synchrotron X-ray powder diffraction measurements confirm the high quality of the MOF nanocrystals when embedded in a hydrophobic polymer such as PU and their improved stability in an aqueous environment, compared to the pure MOF. Although the inner porous structure is not accessible to nitrogen with a quadrupole moment, this is not the case for the adsorption of nonpolar molecules (e.g., hydrocarbons) at room temperature. Although the partial accessibility of the embedded MOFs limits the brimonidine adsorption performance, the UiO-67@PU composite gives rise to a 60-fold improvement compared to the neat PU film. Synchrotron XRPD, TGA, and FTIR measurements of the composite before and after loading brimonidine confirm the presence of the drug within the UiO-67@PU film, although the real role of the polymer matrix and the UiO-67 nanocrystals cannot be conclusively confirmed. The total brimonidine uptake of the composite is as high as $58.4 \text{ mg}_{\text{BRI}}$ per gram of composite or $194.7 \text{ mg}_{\text{BRI}}$ per gram of MOF. These results in the liquid phase are highly promising and open the door for the design of novel polymeric inserts with functional properties and improved performance (for instance, with drug delivery properties) to be applied in a number of ophthalmological disorders, either as a component of contact lens, in the composition of lacrimal stoppers (e.g., punctal plugs), or in subtenon inserts.

■ ASSOCIATED CONTENT

SI Supporting Information

The Supporting Information is available free of charge at <https://pubs.acs.org/doi/10.1021/acsami.0c07517>.

Physicochemical characterization of the synthesized samples (synchrotron X-ray powder diffraction, TGA profiles, and gas adsorption measurements), adsorption kinetics for brimonidine, and mathematical models applied (PDF)

■ AUTHOR INFORMATION

Corresponding Author

J. Silvestre-Albero – Laboratorio de Materiales Avanzados, Departamento de Química Inorgánica-IUMA, Universidad de Alicante, E-03690 San Vicente del Raspeig, Spain; orcid.org/0000-0002-0303-0817; Email: joaquin.silvestre@ua.es

Authors

J. Gandara-Loe – Laboratorio de Materiales Avanzados, Departamento de Química Inorgánica-IUMA, Universidad de Alicante, E-03690 San Vicente del Raspeig, Spain; orcid.org/0000-0003-1334-4788

B. E. Souza – Multifunctional Materials & Composites (MMC) Laboratory, Department of Engineering Science, University of Oxford, Oxford OX1 3PJ, U.K.; orcid.org/0000-0001-6315-2149

A. Missyul – CELLS-ALBA Synchrotron, E-08290 Cerdanyola del Valles, Spain; orcid.org/0000-0002-0577-4481

G. Giraldo – Clínica Clofan, Colombia

J.-C. Tan – Multifunctional Materials & Composites (MMC) Laboratory, Department of Engineering Science, University of Oxford, Oxford OX1 3PJ, U.K.; orcid.org/0000-0002-5770-408X

Complete contact information is available at: <https://pubs.acs.org/doi/10.1021/acsami.0c07517>

Author Contributions

[†]J.G.-L. and B.E.S. contributed equally.

Notes

The authors declare no competing financial interest.

■ ACKNOWLEDGMENTS

The authors would like to acknowledge financial support from MINECO (MAT2016-80285-p), Spanish ALBA Synchrotron (Project 2020014008), and H2020 (MSCA-RISE-2016/NanoMed Project). B.E.S. thanks the Minas Gerais Research Foundation (FAPEMIG CNPJ n21.949.888/0001-83) for a DPhil scholarship award. J.-C.T. thanks the EPSRC (Grant No. EP/N014960/1) and ERC Consolidator Grant (PROMOFS under the grant agreement 771575) for funding.

■ REFERENCES

(1) Hertzog, L. H.; Albrecht, K. G.; LaBree, L.; Lee, P. P. Glaucoma Care and Conformance with Preferred Practice Patterns: Examination of the Private, Community-Based Ophthalmologist. *Ophthalmology* **1996**, *103*, 1009–1013.

(2) Quigley, H. A.; Broman, A. T. The Number of People with Glaucoma Worldwide in 2010 and 2020. *Br. J. Ophthalmol.* **2006**, *90*, 262–267.

(3) Clineschmidt, C. M.; Williams, R. D.; Snyder, E.; Adamsons, I. A. A Randomized Trial in Patients Inadequately Controlled with

Timolol Alone Comparing the Dorzolamide-Timolol Combination to Monotherapy with Timolol or Dorzolamide. *Ophthalmology* **1998**, *105*, 1952–1959.

(4) Le Boultais, C.; Acar, L.; Zia, H.; Sado, P. A.; Needham, T.; Leverage, R. Ophthalmic Drug Delivery Systems—Recent Advances. *Prog. Retinal Eye Res.* **1998**, *17*, 33–58.

(5) Gulsen, D.; Chauhan, A. Ophthalmic Drug Delivery through Contact Lenses. *Invest. Ophthalmol. Vis. Sci.* **2004**, *45*, 2342–2347.

(6) Gaudana, R.; Ananthula, H. K.; Parenky, A.; Mitra, A. K. Ocular Drug Delivery. *AAPS J.* **2010**, *12*, 348–360.

(7) Urtili, A. Challenges and Obstacles of Ocular Pharmacokinetics and Drug Delivery. *Adv. Drug Delivery Rev.* **2006**, *58*, 1131–1135.

(8) De, T. K.; Rodman, D. J.; Holm, B. A.; Prasad, P. N.; Bergey, E. J. Brimonidine Formulation in Polyacrylic Acid Nanoparticles for Ophthalmic Delivery. *J. Microencapsulation* **2003**, *20*, 361–374.

(9) Singh, K. H.; Shinde, U. A. Chitosan Nanoparticles for Controlled Delivery of Brimonidine Tartrate to the Ocular Membrane. *Pharmazie* **2011**, *66*, 594–599.

(10) Prabhu, P.; Nitish Kumar, R.; Koland, M.; Harish, N. M.; Vijayanarayan, K.; Dhondge, G.; Charyulu, R. N. Preparation and Evaluation of Nano-Vesicles of Brimonidine Tartrate as an Ocular Drug Delivery System. *J. Young Pharm.* **2010**, *2*, 356–361.

(11) Sun, J.; Lei, Y.; Dai, Z.; Liu, X.; Huang, T.; Wu, J.; Xu, Z. P.; Sun, X. Sustained Release of Brimonidine from a New Composite Drug Delivery System for Treatment of Glaucoma. *ACS Appl. Mater. Interfaces* **2017**, *9*, 7990–7999.

(12) Ghate, D.; Edelhauser, H. F. Ocular Drug Delivery. *Expert Opin. Drug Delivery* **2006**, *3*, 275–287.

(13) Diebold, Y.; Jarrín, M.; Sáez, V.; Carvalho, E. L. S.; Orea, M.; Calonge, M.; Seijo, B.; Alonso, M. J. Ocular Drug Delivery by Liposome–Chitosan Nanoparticle Complexes (LCS-NP). *Biomaterials* **2007**, *28*, 1553–1564.

(14) Sun, S.; Li, J.; Li, X.; Lan, B.; Zhou, S.; Meng, Y.; Cheng, L. Episcleral Drug Film for Better-Targeted Ocular Drug Delivery and Controlled Release Using Multilayered Poly- ϵ -Caprolactone (PCL). *Acta Biomater.* **2016**, *37*, 143–154.

(15) Saetone, M. F.; Salminen, L. Ocular Inserts for Topical Delivery. *Adv. Drug Delivery Rev.* **1995**, *16*, 95–106.

(16) Brown, H. S.; et al. Visual Effects of Pilocarpine in Glaucoma. *Arch. Ophthalmol.* **1976**, *94*, 1716.

(17) Pollack, I. P.; Quigley, H. A.; Harbin, T. S. The Ocuser System: Advantages and Disadvantages. *South. Med. J.* **1976**, *69*, 1296–1298.

(18) Mehta, P.; Justo, L.; Walsh, S.; Arshad, M. S.; Wilson, C. G.; O'Sullivan, C. K.; Moghimi, S. M.; Vizirianakis, I. S.; Avgoustakis, K.; Fatouros, D. G.; Ahmad, Z. New Platforms for Multi-Functional Ocular Lenses: Engineering Double-Sided Functionalized Nano-Coatings. *J. Drug Targeting* **2015**, *23*, 305–310.

(19) dos Santos, J.-F. R.; Alvarez-Lorenzo, C.; Silva, M.; Balsa, L.; Couceiro, J.; Torres-Labandeira, J.-J.; Concheiro, A. Soft Contact Lenses Functionalized with Pendant Cyclodextrins for Controlled Drug Delivery. *Biomaterials* **2009**, *30*, 1348–1355.

(20) Verestiuc, L.; Nastasescu, O.; Barbu, E.; Sarvaiya, I.; Green, K. L.; Tsiouklis, J. Functionalized Chitosan/NIPAM (HEMA) Hybrid Polymer Networks as Inserts for Ocular Drug Delivery: Synthesis, in Vitro Assessment, and in Vivo Evaluation. *J. Biomed. Mater. Res., Part A* **2006**, *77A*, 726–735.

(21) Sun, C.-Y.; Qin, C.; Wang, X.-L.; Su, Z.-M. Metal-Organic Frameworks as Potential Drug Delivery Systems. *Expert Opin. Drug Delivery* **2013**, *10*, 89–101.

(22) Zhou, H.-C.; Long, J. R.; Yaghi, O. M. Introduction to Metal–Organic Frameworks. *Chem. Rev.* **2012**, *112*, 673–674.

(23) Horcajada, P.; Serre, C.; Vallet-Regí, M.; Sebba, M.; Taulelle, F.; Férey, G. Metal–Organic Frameworks as Efficient Materials for Drug Delivery. *Angew. Chem., Int. Ed.* **2006**, *45*, 5974–5978.

(24) Sun, Y.; Zheng, L.; Yang, Y.; Qian, X.; Fu, T.; Li, X.; Yang, Z.; Yan, H.; Cui, C.; Tan, W. Metal–Organic Framework Nanocarriers for Drug Delivery in Biomedical Applications. *Nano-Micro Lett.* **2020**, *12*, No. 103.

- (25) Gandara-Loe, J.; Ortuño-Lizarán, I.; Fernández-Sánchez, L.; Alió, J. L.; Cuenca, N.; Vega-Estrada, A.; Silvestre-Albero, J. Metal–Organic Frameworks as Drug Delivery Platforms for Ocular Therapeutics. *ACS Appl. Mater. Interfaces* **2019**, *11*, 1924–1931.
- (26) Chavan, S.; Vitillo, J. G.; Gianolio, D.; Zavorotynska, O.; Civalleri, B.; Jakobsen, S.; Nilsen, M. H.; Valenzano, L.; Lamberti, C.; Lillerud, K. P.; Bordiga, S. H₂ Storage in Isostructural UiO-67 and UiO-66 MOFs. *Phys. Chem. Phys.* **2012**, *14*, 1614–1626.
- (27) Lee, V. H. L.; Robinson, J. R. Topical Ocular Drug Delivery: Recent Developments and Future Challenges. *J. Ocul. Pharmacol. Ther.* **1986**, *2*, 67–108.
- (28) Xu, J.; Xue, Y.; Hu, G.; Lin, T.; Gou, J.; Yin, T.; He, H.; Zhang, Y.; Tang, X. A Comprehensive Review on Contact Lens for Ophthalmic Drug Delivery. *J. Controlled Release* **2018**, *281*, 97–118.
- (29) Rodenas, T.; Luz, I.; Prieto, G.; Seoane, B.; Miro, H.; Corma, A.; Kapteijn, F.; Llabrés i Xamena, F. X.; Gascon, J. Metal–Organic Framework Nanosheets in Polymer Composite Materials for Gas Separation. *Nat. Mater.* **2015**, *14*, 48–55.
- (30) Mahdi, E. M.; Tan, J.-C. Mixed-Matrix Membranes of Zeolitic Imidazolate Framework (ZIF-8)/Matrimid Nanocomposite: Thermo-Mechanical Stability and Viscoelasticity Underpinning Membrane Separation Performance. *J. Membr. Sci.* **2016**, *498*, 276–290.
- (31) Souza, B. E.; Donà, L.; Titov, K.; Bruzzese, P.; Zeng, Z.; Zhang, Y.; Babal, A. S.; Möslin, A. F.; Frogley, M. D.; Wolna, M.; Cinque, G.; Civalleri, B.; Tan, J.-C. Elucidating the Drug Release from Metal–Organic Framework Nanocomposites via In Situ Synchrotron Microspectroscopy and Theoretical Modeling. *ACS Appl. Mater. Interfaces* **2020**, *12*, 5147–5156.
- (32) Katz, M. J.; Brown, Z. J.; Colón, Y. J.; Siu, P. W.; Scheidt, K. A.; Snurr, R. Q.; Hupp, J. T.; Farha, O. K. A Facile Synthesis of UiO-66, UiO-67 and Their Derivatives. *Chem. Commun.* **2013**, *49*, 9449.
- (33) Denny, M. S., Jr.; Cohen, S. M. In Situ Modification of Metal–Organic Frameworks in Mixed-Matrix Membranes. *Angew. Chem., Int. Ed.* **2015**, *54*, 9029–9032.
- (34) Mahdi, E. M.; Tan, J.-C. Dynamic Molecular Interactions between Polyurethane and ZIF-8 in a Polymer-MOF Nanocomposite: Microstructural, Thermo-Mechanical and Viscoelastic Effects. *Polymer* **2016**, *97*, 31–43.
- (35) Karamanos, N. K.; Lamari, F.; Katsimpris, J.; Gartaganis, S. Development of an HPLC Method for Determining the Alpha2-Adrenergic Receptor Agonist Brimonidine in Blood Serum and Aqueous Humor of the Eye. *Biomed. Chromatogr.* **1999**, *13*, 86–88.
- (36) Bastani, D.; Esmaili, N.; Asadollahi, M. Polymeric Mixed Matrix Membranes Containing Zeolites as a Filler for Gas Separation Applications: A Review. *J. Ind. Eng. Chem.* **2013**, *19*, 375–393.
- (37) Mahdi, E. M.; Cuadrado-Collados, C.; Silvestre-Albero, J.; Tan, J.-C. Polymer Nanocomposites Functionalised with Nanocrystals of Zeolitic Imidazolate Frameworks as Ethylene Control Agents. *Mater. Today Adv.* **2019**, *2*, 100008.
- (38) Trovati, G.; Sanches, E. A.; Neto, S. C.; Mascarenhas, Y. P.; Chierice, G. O. Characterization of Polyurethane Resins by FTIR, TGA, and XRD. *J. Appl. Polym. Sci.* **2010**, *115*, 263–268.
- (39) Ball, D. W.; Hill, J. W.; Scott, R. J. *The Basics of General, Organic, and Biological Chemistry*; Saylor, 2011.
- (40) Bao, Z.; Wang, J.; Zhang, Z.; Xing, H.; Yang, Q.; Yang, Y.; Wu, H.; Krishna, R.; Zhou, W.; Chen, B.; Ren, Q. Molecular Sieving of Ethane from Ethylene through the Molecular Cross-Section Size Differentiation in Gallate-based Metal–Organic Frameworks. *Angew. Chem., Int. Ed.* **2018**, *57*, 16020–16025.
- (41) ul Qadir, N.; Said, S. A. M.; Bahaidarah, H. M. Structural Stability of Metal Organic Frameworks in Aqueous Media – Controlling Factors and Methods to Improve Hydrostability and Hydrothermal Cyclic Stability. *Microporous Mesoporous Mater.* **2015**, *201*, 61–90.
- (42) Lawrence, M. C.; Schneider, C.; Katz, M. J. Determining the Structural Stability of UiO-67 with Respect to Time: A Solid-State NMR Investigation. *Chem. Commun.* **2016**, *52*, 4971–4974.
- (43) DeCoste, J. B.; Peterson, G. W.; Jasuja, H.; Glover, T. G.; Huang, Y.; Walton, K. S. Stability and Degradation Mechanisms of Metal–Organic Frameworks Containing the Zr₆O₄(OH)₄ Secondary Building Unit. *J. Mater. Chem. A* **2013**, *1*, 5642.
- (44) Mondloch, J. E.; Katz, M. J.; Planas, N.; Semrouni, D.; Gagliardi, L.; Hupp, J. T.; Farha, O. K. Are Zr₆-Based MOFs Water Stable? Linker Hydrolysis vs. Capillary-Force-Driven Channel Collapse. *Chem. Commun.* **2014**, *50*, 8944.
- (45) Chandak, A. R.; Verma, P. R. P. Development and Evaluation of HPMC Based Matrices for Transdermal Patches of Tramadol. *Clin. Res. Regul. Aff.* **2008**, *25*, 13–30.
- (46) Aburahma, M. H.; Mahmoud, A. A. Biodegradable Ocular Inserts for Sustained Delivery of Brimonidine Tartarate: Preparation and In Vitro/In Vivo Evaluation. *AAPS PharmSciTech* **2011**, *12*, 1335–1347.
- (47) De Souza, J. F.; Maia, K. N.; De Oliveira Patrício, P. S.; Fernandes-Cunha, G. M.; Da Silva, M. G.; De Matos Jensen, C. E.; Da Silva, G. R. Ocular Inserts Based on Chitosan and Brimonidine Tartrate: Development, Characterization and Biocompatibility. *J. Drug Delivery Sci. Technol.* **2016**, *32*, 21–30.
- (48) Dias, R. C. M.; Góes, A. M.; Serakides, R.; Ayres, E.; Oréfice, R. L. Porous Biodegradable Polyurethane Nanocomposites: Preparation, Characterization, and Biocompatibility Tests. *Mater. Res.* **2010**, *13*, 211–218.
- (49) Seymour, R. W.; Cooper, S. L. Thermal Analysis of Polyurethane Block Polymers. *Macromolecules* **1973**, *6*, 48–53.
- (50) Zhu, X.; Li, B.; Yang, J.; Li, Y.; Zhao, W.; Shi, J.; Gu, J. Effective Adsorption and Enhanced Removal of Organophosphorus Pesticides from Aqueous Solution by Zr-Based MOFs of UiO-67. *ACS Appl. Mater. Interfaces* **2015**, *7*, 223–231.
- (51) Pankajakshan, A.; Sinha, M.; Ojha, A. A.; Mandal, S. Water-Stable Nanoscale Zirconium-Based Metal–Organic Frameworks for the Effective Removal of Glyphosate from Aqueous Media. *ACS Omega* **2018**, *3*, 7832–7839.
- (52) Maiti, S.; Paul, S.; Mondol, R.; Ray, S.; Sa, B. Nanovesicular Formulation of Brimonidine Tartrate for the Management of Glaucoma: In Vitro and In Vivo Evaluation. *AAPS PharmSciTech* **2011**, *12*, 755–763.
- (53) Kim, S.-N.; Park, C. G.; Huh, B. K.; Lee, S. H.; Min, C. H.; Lee, Y. Y.; Kim, Y. K.; Park, K. H.; Choy, Y. B. Metal–Organic Frameworks, NH₂-MIL-88(Fe), as Carriers for Ophthalmic Delivery of Brimonidine. *Acta Biomater.* **2018**, *79*, 344–353.
- (54) Emad Eldeeb, A.; Salah, S.; Ghorab, M. Proniosomal Gel-Derived Niosomes: An Approach to Sustain and Improve the Ocular Delivery of Brimonidine Tartrate; Formulation, in-Vitro Characterization, and in-Vitro Pharmacodynamic Study. *Drug Delivery* **2019**, *26*, 509–521.